Cutting out Cobalt: Cathode Alternatives

Amanda Siciliano, Daniela Fontecha, Alex Hall

Group Contributions: All three members were involved in the writing and editing of group sections including Introduction (section 1), Proposal and Experimental Validation (section 5), and Conclusion (section 6). For individual contributions, Amanda is the primary author of Stabilization of Crystal Structures (section 2), Alex is the primary author of Carbon Enhanced Nanoconfinement/Tunneling (section 3), and Daniela is the primary author of Doping of Metal Fluorides for Enhanced Cathode Performance (section 4).

1. Introduction: Cobalt and Applications

1.1 Mining History & Constraints

Cobalt ranks as the 31st most abundant element in the Earth's crust at approximately 0.003%, and the 41st most abundant element in ocean water at approximately 8e-9%[1]. Because free cobalt does not occur naturally, it is mainly refined as a byproduct of copper and nickel mining in the Democratic Republic of the Congo (DRC). Nearly 70% of cobalt comes from the DRC, with over 20% of the supply coming from smaller, artisanal mines[2]. Even though cobalt has provided a source of livelihood for citizens in this poor, war-torn country, many of the artisanal mines use poor working conditions and child labor, with workers exposed to fatal diseases from the absence of basic protective personal equipment[2].

Despite international rulings holding governments accountable for protecting and eliminating child labor, many of the mines continue to exploit children throughout all steps of the mineral's supply chain[2]. In response, International Rights Advocates, a non-governmental organization, filed a federal class action lawsuit against several companies that profit from the poor working conditions necessary to mine cobalt[3]. Although cobalt is a necessary material, access to cobalt as an endangered element with geopolitical conflicts will continue to diminish over time.

1.2 Elemental Properties

Cobalt is a brittle, hard transition metal with ferromagnetic properties. It is a favorable material with countless applications because of its hard wearing, high corrosion resistance, and high melting point of nearly 1500 °C[1]. The crystal structure of cobalt is temperature and grain size dependent, where the element is most thermodynamically stable in a face-centered cubic (FCC) crystal structure above 450 °C and in a hexagonal close-packed (HCP) crystal structure below 450 °C[4].

Mechanical processes cause transformations of the crystal structure, creating alloys with favorable phase transition properties. In the milling process, balls that transfer energy to the powder particles cause a buildup of defects in the lattice structure, inhibiting an allotropic transformation[5]. As a result, the grain size is reduced to a nanoscale and the element undergoes a transformation. Because grain size alters specific properties such as saturation magnetization, chemical composition, and curie temperature, their quantum size improves magnetic, electrical, mechanical, and optical properties.

The alloys created from mechanical processes can vary greatly in properties, depending on the composition of elements involved. Nickel cobalt alloys are superior in applications where high tensile, yield strength, and ductility are needed. As cobalt content increases, there is a change in crystal structure from FCC to HCP, along with a zone of co-existence between the two crystal structures in alloys with 50-80% cobalt composition, leading to amplified covalent bonding between the cobalt and nickel atoms[6]. Cobalt chromium alloys are superior in applications where

high corrosion resistance, and temperature strength are needed. These alloys have strength properties similar to stainless steel, but are superior because of their wear resistance[7].

1.3 Societal Functions

Corrosion resistance and high strength properties of cobalt alloys are favorable for aircraft engines and biomedical fixation devices alike, but the primary use of cobalt is for rechargeable batteries. China is the world's largest importer of cobalt, with over 80% of material consumption used for rechargeable batteries[8]. Because of cobalt's usage as a cathode material within rechargeable lithium-ion batteries (LIBs), demand is expected to double by 2030, reaching an estimated demand range of 259 to 474 tons[9].

With the development of technology, there is a huge push in both the consumer electronics and electric vehicle markets. Consumer electronics companies, such as Samsung, Apple, and Bose, dominate the 1 trillion USD market, which is expected to grow at a 7% compound annual growth rate from 2020 to 2026[10]. Automotive companies, such as Tesla, BMW, and Nissan, dominate the electric vehicle market, which is expected to grow at a 21.2% compound annual growth rate from 2020 to 2030 because of the push towards sustainability[11].

Two companies were examined for their work in removing cobalt from LIBs: Sila Nanotechnologies and TexPower. Sila Nanotechnologies is a startup company focused on advanced electrode materials. Their contributions to advancing electrode research serves as a large inspiration for this project. One of Sila's co-founders, Dr. Gleb Yushin, has continuously innovated the use of nanostructured materials in cathodes over the last ten years. TexPower is also a startup company focused on eliminating cobalt from cathode materials. Co-founder Dr. Wangda Li attributed TexPower's success to the group's combined experience, where Li has strong connections to Dr. John Goodenough. Upon Goodenough's discovery of the modern LIB, cobalt has been the favored material within cathodes for rechargeable batteries.

1.4 Cobalt in Lithium-Ion Batteries

Cobalt is most used in LIBs as lithium cobalt oxide ($LiCoO_2$), which is an intercalation cathode material in which lithium ions are inserted into the interplanar layers of the cathode during the discharge of the battery as shown in **Figure 1.4 a**. In the 1980's the stability of $LiCoO_2$ during lithiation and delithiation was realized, leading to the boom of rechargeable LIBs[12]. Other metal oxides and sulfides have been investigated, but none have shown comparable cyclability or discharge capacity. The reason $LiCoO_2$ works so well in this application is partly due to the large spacing between cobalt oxide layers, larger than in any other lithium metal oxides (Li_xMO_2). Additionally, the cobalt containing Li_xMO_2 configuration has the high electron affinity of the low spin Co +3/+4, strongly polarizing the oxygen layers and leaving lithium more free to move. Most Li_xMO_2 compounds were found to have good electrical conductivities owed to their small band gaps (**Figure 1.4 b**), and $LiCoO_2$ is no exception.

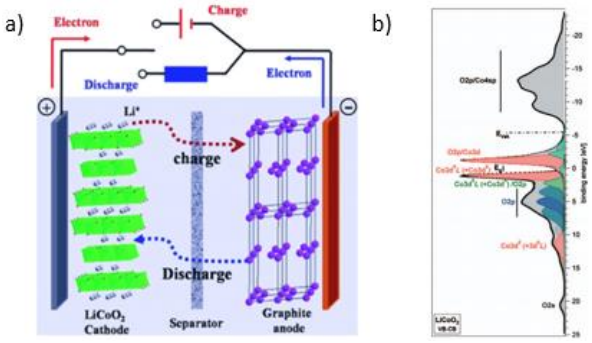

Figure 1.4: a) A schematic of a $LiCoO_2$ cathode in a battery from the Royal Chemistry Society.
b) Experimental density of electronic states in $LiCoO_2$ from Ensling et al. 2010 (left to right)

There is much work being done to remove $LiCoO_2$ from batteries, not just to remove cobalt, but to create more powerful batteries. $LiCoO_2$ cathodes, while very stable, are not high in energy density. During charge and discharge cycles, the cobalt atoms in the cathodes only change between the +3 and +4 oxidation states. It would be more efficient to take advantage of many oxidation states of a transition metal. This is the driving force behind conversion cathode research.

1.5 Conversion Cathodes: Metal Fluorides as Alternative to Cobalt-Based Cathodes

Conversion cathodes are an alternative approach to cathode materials that differ from the intercalation mechanism of the $LiCoO_2$ cathode. Instead, conversion cathodes undergo oxidation and reduction reactions, breaking and creating bonds during lithiation and delithiation[13]. One of the primary benefits of conversion cathodes is that all the oxidation states of the transition metal are used, enabling a single metal atom to sustain multiple lithium ions when fully lithiated, thus increasing the energy density of the battery[14]. A wide array of abundant and inexpensive elements is seen in conversion cathodes, with their theoretical capacities and potentials in **Figure 1.5.1**[13].

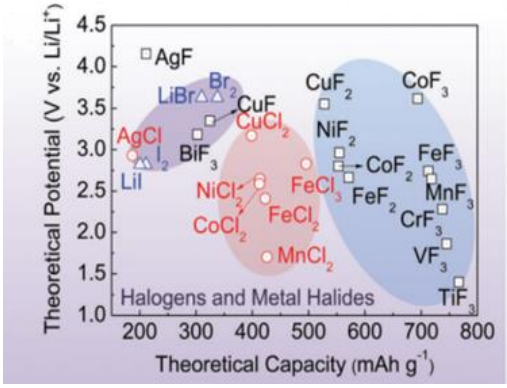

Figure 1.5.1: Theoretical capacities and theoretical potential of conversion cathodes that are composed of chalcogenides[13].

Figure 1.5.1 shows that metal fluorides (MFs) have the potential to produce high capacities and voltages, depending on composition[13]. Metal fluorides are a promising alternative to $LiCoO_2$ because their high ionic character allows for high operating voltages. However, the strong ionic M-F bond also leads to issues with conductivity in practice. Iron (III) fluoride (FeF_3) demonstrates the ability to function at high temperatures, which is crucial when considering its application as a cathode material for LIBs[14]. Taking sustainability and cost into account, FeF_3 is a good choice of metal fluoride since iron is the 4th most abundant element on Earth's crust and is very inexpensive while also exhibiting low toxicity[15].

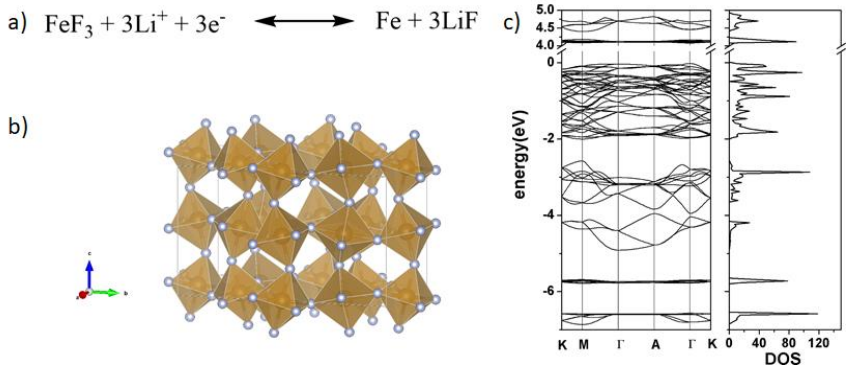

Figure 1.5.2. a) The redox reaction that an FeF_3 cell cathode undergoes upon charging and discharging of the cell[13] b) Rhombohedral FeF_3 supercell crystal structure c) FeF_3 electronic band structure (left) and density of states (right)[16].

This paper will discuss only true conversion cathodes, in which the lithiation reaction goes to completion to form a two-phase nanocomposite composed of Li-halide and the reduced metal (**Figure 1.5.2a**). FeF_3 is a true conversion cathode with a rhombohedral crystalline structure (**Figure 1.5.2b**) undergoing a redox reaction in which iron is fully reduced to Fe^0 and LiF forms during lithiation[13]. The most stable form of FeF_3 is

antiferromagnetic FeF_3 and its band structure is shown in **Figure 1.5.2c**. It is evident that the bandgap of ~4.0 eV is the cause of the low conductivity that results from FeF_3 cathodes[16].

Despite the promising high operational voltage, theoretical capacity, and energy density of FeF_3 cathodes, their ability to remain stable is limited by several factors. In addition to its large bandgap, conversion cathodes experience large volume changes upon lithiation due to FeF_3 being able to accommodate multiple lithium ions per metal site. When reduced, iron also aggregates, which makes the redox reaction irreversible over time[13]. The following sections will address how the challenges of FeF_3 as a cathodic material can be overcome.

2. Stabilization of Crystal Structures (Primary Author: Amanda P. Siciliano)

Stable crystal structures in transition-metal fluorides enhance capacity retention and create strong cathodes, allowing batteries to remain powerful after many charging and discharging cycles. While $LiCoO_2$ is an attractive cathode material, it allows for only one lithium ion bonding site, thus limiting the energy density of electron transfer. As a result, transition-metal conversion cathodes that permit lithium ions to have more than one bonding site per metal are desired, as they will enable higher energy densities. After selecting iron fluoride (FeF_3) as the desired conversion cathode candidate, it is important to analyze different ways to stabilize the crystal structure. Doping and nanoconfinement are two different ways to explore stabilization, with techniques such as X-ray diffraction (XRD), Vienna ab-initio simulation package (VASP), electron diffraction (ED), density functional theory (DFT), selected area electron diffraction patterns (SAED), and being used to understand changes in the crystal structure.

Mesoporous FeF_3 cathodes, which are created through a novel non-aqueous synthesis, found that the hexagonal-tungsten-bronze (HTB)-phase FeF_3 hydrate complexes ($FeF_3 \cdot 0.33H_2O$) improved lithium storage capacity[17]. However, because this composite still experienced issues with cycling, doping was explored as another method to stabilize the crystal structure. As a result, several different metals, including titanium, iron, manganese, and cobalt have been examined for their structural changes upon doping with FeF_3 containing minute amounts of crystalline water. Heterovalent substitution, a synthesis strategy that involves doping valence electrons with impurities, is believed to improve the material conductivity. When material structure is altered through the increasing of space cavities and the lowering of bandgap - which is discussed in section 4 - charge adjustment, and thus material conductivity, will be enhanced[18].

In research that examined Ni-doped $FeF_3 \cdot 0.33H_2O$, results indicated the potential for rapid ion transport increased as the crystal structure stabilized from lattice expansion. Ni-doped $FeF_3 \cdot 0.33H_2O$ XRD patterns showed that, because there were no newly formed characteristic peaks, nickel atoms were fully immersed within the host $FeF_3 \cdot 0.33H_2O$. Further analysis of characteristic XRD peaks revealed a slight lowering in peak angle, indicating that the larger nickel ion effectively entered the host lattice. The lattice parameters, and thus lattice volumes, of the doped crystal lattice, 0.71237 nm^3 , increased slightly when compared to the undoped crystal lattice, of 0.71234 nm^3. This increase in lattice volume concurs with earlier results, and confirms the enhanced transport of ions, electrons, and electrolytes through the stabilization of an enlarged crystal structure[19].

Similar findings are present in research by Yang et al. (2016)[20] which investigates the effect of metal doping on properties of $FeF_3 \cdot 0.33H_2O$ through first principle calculations. These calculations used the total-energy and molecular-dynamics package VASP. In optimizing the crystal structure, a similar result to Liu et al. (2020)[19] was discovered, where the lattice parameters and lattice volume increased when comparing the crystal structures volumes of undoped $FeF_3 \cdot$

$0.33H_2O$, 0.713065 nm^3, and Ti-doped $FeF_3 \bullet 0.33H_2O$, 0.716028 nm^3. Because of the larger radius of the Ti+3 ions, 0.67 nm, in comparison to the radius of Fe+3 ions, 0.645 nm, the crystal volume expands. This expansion in the lattice creates a larger cavity, permitting enhanced transport of lithium ions. The hexagonal cavity, as shown in **Figure 2.1**, compares $FeF_3 \bullet 0.33H_2O$ (a) with various proportions of Ti-doped $FeF_3 \bullet 0.33H_2O$ (b, c, d). As a result, it was discovered that Ti-doping can increase the FeF_3 cavity size, expanding lithium charge and discharge cycling. The $FeF_3 \bullet 0.33H_2O$ crystal structure was stabilized by allowing for open lithium-ion diffusion, which enhanced electronic and ionic conductivity. While this method was found to improve lithium-ion cycling, issues relating to reduced metal aggregation and irreversibility still exist[20].

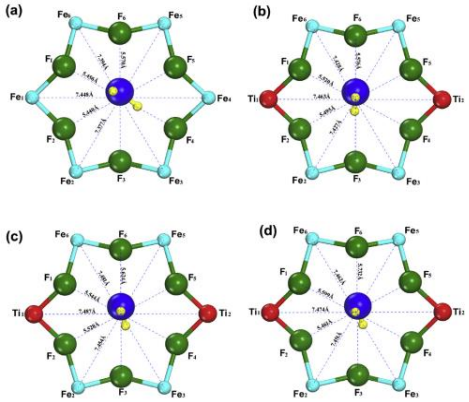

Figure 2.1: Hexagonal cavities in various $FeF_3 \bullet 0.33H_2O$ structures (a) $FeF_3 \bullet 0.33H_2O$ (b) $Ti_{0.08}Fe_{0.92}F_3 \bullet 0.33H_2O$ (c) $Ti_{0.17}Fe_{0.83}F_3 \bullet 0.33H_2O$ (d) $Ti_{0.25}Fe_{0.75}F_3 \bullet 0.33H_2O$[20].

Nanoconfinement is another method for enhancing crystal structure. Upon exploring the lithiation conversion reaction of FeF_3 nanoparticles confined with carbon films, it was discovered that lithium ion transport occurs at two different speeds. Because of diffusion along carbon films, lithium ions move quickly along the FeF_3 surfaces, and much slower after penetrating the bulk material. An immediate decomposition reaction blocks the iron from diffusing within the lithium fluoride (LiF), resulting in an increase to the volume of the iron nanoparticles as the low-density LiF fills the surrounding space. As the volume increases, a structural shift occurs, and the lattice expands. This structural evolution of FeF_3 nanoparticles is shown through ED, where iron (110) peaks do not shift in position because of lithiation but rather change in angle, as shown in **Figure 2.2**. The enlarged view, shown in **Figure 2.2c**, displays a red dashed line which was created through peak position and intensity fitting. The increase in peak angles indicates a lattice expansion that moves from the bulk towards the surface, as iron nanoparticles grow upon nucleation[21].

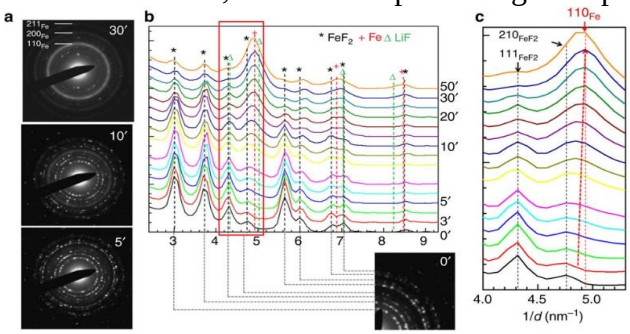

Figure 2.2: (b) ED pattern characteristic intensity peaks showing an enlarged view (c) of the growth of the angle of iron peaks upon lithiation[21].

As the lithium directly intercalates into the bulk FeF_3, amorphization occurs as a recrystallization process supersaturates the crystal structure. The new crystallographic orientation from redistribution of iron and fluoride ions causes the combined structure to decompose at slower rates, which is confirmed through DFT and phase-field simulations. A new pathway for ion transport is created within the nanoparticles, allowing for the slower electrochemical conversion reactions in the bulk material to form finely-sized phase formations through a layered propagation process. These finely-sized nanophase formations will alter charge and discharge cycles and provide an opportunity to develop high-energy conversion electrodes[21].

Another means of stabilizing the FeF_3 crystal structure lies within examining the conversion process for positive electrodes. Finding an electrode with higher energy density, and thus higher specific capacity, has been accomplished by exploring various oxidation states. Through the use of carbon metal fluoride nanocomposites (CMFNCs) and electrically connected grains, the electrochemical activity of FeF_3 was observed to have a 99% recovery capacity. Metal fluorides, which are typically not favored cathode materials because of large bandgaps, saw reductions in crystal structure size. This reduced size occurred through enhancements to the electronic and ionic activity, as the volume along the defect-filled surface increased. Through SAED, which determines the structures of phases present, it was determined that even though carbon fluoride compounds were formed, they play no role in overall electrochemical activity. Structural characterization techniques, including XRD which was used to characterize material structure, confirm the development of (110) FeF_3 peaks in recovered samples. As a result, it is confirmed that FeF_3 nanocomposites reform with finer structures[22].

3. Carbon Enhanced Nanoconfinement / Tunneling (Primary Author: Alex Hall)

Crystalline FeF_3 cathodes dissolve quickly in conventional liquid organic electrolytes. There are different methods to tackle this; some work is being done to create mixed intercalation/conversion metal fluoride cathodes. This provides both added stability and energy density, but still leaves some energy density on the table. This section will focus on nanoconfinement to boost stability and electronic conductivity of FeF_3 based cathodes.

If one can overlook or overcome the dissolution problem, conversion cathodes in general are typically plagued by large volume changes during cycling (compared to more traditional intercalation type cathodes)[13]. This causes the whole cell to become unstable, combined with a flammable organic liquid electrolyte and the potential for short circuits, the result is a large fire hazard.

Many studies into confining these metal fluorides have been done, largely focusing on carbon (carbon black, graphite, etc.) for beneficial electron transport properties (to be discussed later). The nanostructures used for confinement are numerous, including carbon nanocomposites, nanotubes, and nanofibers. Nanocomposite studies show faster lithiation as the lithium ions in the electrolyte do not have to penetrate the bulk FeF_3 crystal structure (which to add to its low electrical conductivity, has similar problems with ionic conductivity)[21]. Instead, the lithium can move in the space between spherical nanocomposite particles. This technique also reduces some of the issues surrounding metal and LiF aggregation. Aggregation still occurs, but it is spread through the cathode more evenly, rather than only occurring in the interface between electrolyte and cathode.

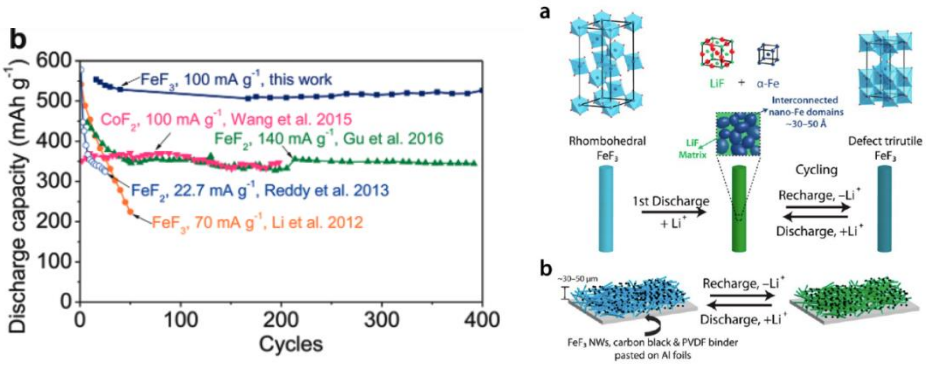

Figure 3.1: The left figure demonstrates the discharge capacity retention achieved by Fu et al[24]. The right shows the structures of FeF_3 nanowires during charge and discharge cycles as demonstrated by Li, Meng, & Jin[23].

Carbon nanotubes (CNT) filled with metal fluoride nanoparticles have also shown some interesting results. As a cathode, metal fluoride CNTs are quite stable even at high voltages. This stability allows the use of a lithium metal anode, the holy grail of battery research since it has the highest theoretical potential. This also requires rethinking the electrolyte, which needs to be stable against lithium metal. It may prove very fruitful in the future, but currently a more "plug and play" approach to removing cobalt is needed.

Free standing FeF_3 nanowire (NW) cathodes have been constructed[23]. These demonstrated a high initial discharge capacity due to the nanostructure's interaction with lithium in the electrolyte, but quickly deteriorated (Figure 3.1, right). The capacity boost comes from the increased surface area of the NW relative to ~150 nm crystalline FeF_3 domains. Since lithium does not need to penetrate the bulk, reaction kinetics are enhanced. Free standing FeF_3 NW cathodes demonstrate some of the key problems conversion type cathodes have with electron transfer. During cycling the charge transfer resistance (R_{ct}) increased from an initial 8.9 to 23.6 Ohms after just 50 cycles[23]. The increase was attributed to the buildup of LiF and degradation of the nanowires. Clearly, any work that can lower (and/or stabilize) R_{ct} would be welcomed.

This brings the discussion to metal fluorides confined in carbon nanofibers, which work with industry standard liquid organic electrolytes (even with their flaws) and lithiated graphite anodes. By embedding metal atoms into electrospun carbon nanofibers then fluorinating them (with gaseous NF_3), improved cycling stability and discharge capacity are observed[24] (Figure 3.1, left).

A lingering problem with metal fluoride cathodes is their low electrical conductivity, some qualitative information is presented in Table 1. The problem is largely due to the more ionic nature of the fluoride bonds[22]. An electron dense cathode is all well and good, but if it cannot rapidly share charge carriers, it won't be all that useful. Nanoconfinement has also been shown to alter charge transport, depending on how the metal fluorides are confined.

Early work theorized that metal aggregation in the cathodes could boost the overall conductivity since crystalline FeF_3 and most other metal fluorides are insulators, with substantial band gaps. Hopes were dashed when researchers quickly realized that any conductivity benefits would be irrelevant if the cathode dissolved.

Materials	Electronic conductivity (S m^{-1})	Theoretical potential (V)	Theoretical volume expansion (%)	Experimentally observed voltage hysteresis (V *vs.* Li)	Qualitative solubility in typical organic electrolytes
FeF_2	Insulator[35,39]	2.66	16.7	0.5–1.0[34,88–90]	Cation dissolution[88,89]
FeF_3	Insulator[35,39]	2.74	25.6	0.8–2.0[48–51]	Cation dissolution
CoF_2	Poor[32,39]	2.80	21	0.8–2.0[32,45]	Cation dissolution[32]
CuF_2	Poor[39,40]	3.55	11.6	0.8–1.0[40,46,90]	Cation dissolution[40,90]
NiF_2	Insulator[35,39]	2.96	28.3	1.0–2.0[52,53]	Cation dissolution
BiF_3	Insulator[35,39]	3.18	1.76	0.4–1.5[47,74]	Cation dissolution[74]
LiF	Insulator[26,39]	—	—	—	Partially soluble

Table 1: Compiled properties of metal fluorides, typically insulators which readily dissolve in organic electrolytes.

The concept of embedding metal fluoride nanoparticles in carbon nanofibers is simple enough. While the nanoparticles may not be conductive, the carbon matrix surrounding them is. The conductivity boost has been demonstrated in previous studies using graphene sheets. Embedding FeF_3 water complexes ($FeF_3 \bullet 0.33H_2O$) in graphene sheets lowers the charge transfer resistance from 245.6 to 150.2 Ohms[25]. This is almost entirely due to the excellent electronic conductivity of graphene. The discharge capacity of the $FeF_3 \bullet 0.33H_2O$ cathode isn't that high, but the resistivity improvements should be easy to implement in other kinds of nanostructures, such as nanofibers.

Tunneling phenomena can also be studied in confined nanoparticles. If electrons are able to tunnel between the conducting matrix and the enclosed nanoparticles, the charge transfer resistance should be significantly lower.

Kwon et al. (2002)[26] summarize some common features of nanocrystalline cathodes: They work better when the first electrochemical step is insertion of Li^+. At the first Li^+ insertion step, a higher insertion voltage can be observed at the same insertion level compared to well-crystalline homologues. After the first Li^+ insertion step, the following cycles are reversible enough.

Based on this, an "electrochemical grafting" model (Figure 3.2, left) was proposed[27]. The model proposed a shift of the valence and conduction band edges at the surface of the nanoparticles arising from dangling bonds and surface defects after lithium is first inserted.

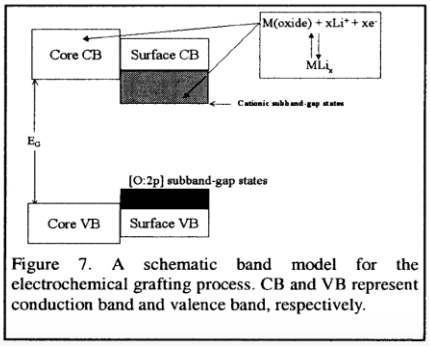

Figure 7. A schematic band model for the electrochemical grafting process. CB and VB represent conduction band and valence band, respectively.

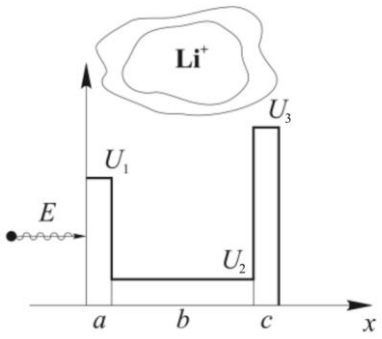

Figure 3.2: The "electrochemical grafting" model as proposed by Kwon et al. (2002)[26] is shown left. Electron tunneling model in 1D nanoparticles as proposed in Lukiyants et al. (2011)[27] right.

The implications of the model were studied in confined SiO_2 as a stand-in for any cathode material nanoconfined in carbon[27]. Confined nanoparticle size was shown to be tied to the specific discharge capacity of constructed cells (Table 2) and was mainly attributed to surface effects. In this specific case, 9 nm nanoparticles were found to maximize the flow of the discharge reaction.

	SiO_2 with average size of particles 16 nm	SiO_2 with average size of particles 11 nm	SiO_2 with average size of particles 9 nm	SiO_2 with average size of particles 5 nm	Macro-structured MnO_2 (theory) [10]	Macro-structured CF_x (theory) [10]
specific capacity, mA·hour/g	648	1080	1890	324	310	860

Table 2: Effect of nanoparticle size on discharge capacity as observed by Lukiyanets et al. (2011).

To better understand these effects, new 1D and 2D models were constructed. The one-dimensional case resembles a particle in a box type situation and is the simplest to interpret (Figure 3.2, right). The lithium nanoparticle (which the electron is tunneling into) is represented by U_2 and the hollows between the nanoparticle and its confining walls are represented by U_1 and U_3. This model gives a prediction of the energy needed for tunneling from either side. The results of the 2D model are similar and the authors conclude that the degree of electron tunneling into a "hollow" is determined by the geometry of the nanopore and the energy of the incident electron. Using these findings, an impedance model is proposed. By constructing equivalent circuit diagrams, the charge transfer resistance can be estimated and optimized by changing the size of the particles. The findings should also translate over to confined metal fluoride nanoparticles.

Using these principles, new research into confinement of metal fluoride nanoparticles can be proposed. Based on the operating potential of the proposed battery cells, optimization of confined metal fluoride nanoparticle size can be performed. Electrochemical impedance spectroscopy can then be used to determine the charge transfer resistance of cells containing different sizes of nanoparticles in the cathode.

4. Doping of Metal Fluorides for Enhanced Cathode Performance (Primary Author: Daniela Fontecha)

As mentioned in section 1.5, FeF_3 cathodes suffer from a low ionic conductivity due to the strong ionic character of the Fe-F bond. This leads to a large bandgap of the material, contributing to electron transport resistance in the cathode as well as requiring high energy to break the Fe-F bond and form LiF in the oxidation reaction[20,28,19].

To take full advantage of the previously mentioned properties that make FeF_3 a promising candidate, other strategies can be implemented to address the low ionic conductivity. In addition to nanoconfinement with CNFs discussed in section 3, which addresses the volumetric change in the cathode as well as enhanced conductivity due to proximity to nanometer thin conductive carbon, strategies to adjust the bandgap of FeF_3 by doping with transition metals have been independently studied[19,20]. It is well documented that introducing dopants to an ionic crystal can reduce its band gap depending on the relative size, electronic structure, and concentration of the dopant. When introducing a dopant, the electrons bound to those atoms overlap until an energy band is formed, called the impurity band. With the right dopant, the impurity band lies between the valence band and conduction band of the pure ionic crystal, lowering the overall bandgap[29].

There are many approaches to modeling the effects of a dopant on a material such as FeF_3. Density functional theory (DFT) is a common method used to describe the electronic structure of periodic systems by accounting for contributions to the ground-state energy of the system with different functionals. The projector augmented wave (PAW) method is a modification to DFT that

generates the pseudo potential to describe the electron density for a given structure. In the case of the structures discussed in this paper, the generalized gradient approximation (GGA) is used, which is an exchange correlation energy approximation that takes into account the electron self-interactions and electron spin density of the system. Additionally, for transition metals an extra correction term should be considered for the electron-electron interactions in the d-orbitals, amounting to a GGA+U calculation. All the calculations discussed below use the Vienna Ab initio Simulation Package (VASP) with the PAW method and GGA+U[20,14,19].

This kind of work has been performed in the past, namely with FeF_3 hydrate complexes ($FeF_3 \bullet nH_2O$) due to the hydrated structure resulting in higher specific capacities and discharge voltages (relative to FeF_3). This stability is attributed to structural integrity that the water molecules provide during the electrochemical reaction while cycling[20,19]. The most stable ferric fluoride hydrate is $FeF_3 \bullet 0.33H_2O$, which has a hexagonal tungsten bronze (HTB) structure. Although the standard FeF_3 structure is rhombohedral instead of HTB, a lot can be learned from the modeled effects of dopants on the $FeF_3 \bullet 0.33H_2O$ structure.

Yang et. al. (2016)[20] performed a computational study of Ti doping on $FeF_3 \bullet 0.33H_2O$. The Ti doping was performed at various concentrations of Ti to test the limits of dopant concentration on the band structure. **Figure 4.1** demonstrates the results of these calculations where a and b represent the undoped band structure and density of states (DOS), e and f represent the highest dopant concentration band structure and DOS and c and d represent intermediate dopant concentrations with the red lines on the band structures representing the fermi energy. The undoped band structure of $FeF_3 \bullet 0.33H_2O$ shows a bandgap of 0.78 eV, which is then decreased to 0.66 and 0.61 eV respectively with increased concentration of Ti in $Fe_xTi_yF_3 \bullet 0.33H_2O$. After further doping, the bandgap is reduced even more and the doped crystal behaves more like a half-metal, thus improving its conductivity. The spin-polarized DOS for the undoped system (**Figure 4.1b**), with the vertical red line representing the fermi energy, shows a sizable gap of about 0.78 eV before reaching the conduction band. **Figure 4.1f** shows the heavily doped system with the up-spin Ti impurity bands (in red) as low in energy as the fermi band and the down-spin impurity bands at 0.5 eV - explaining the half-metal behavior. While half-metal behavior is not the desired result of doping metal fluorides, it is useful to understand the limits of doping on improving the conductivity for cathodic materials applications[20].

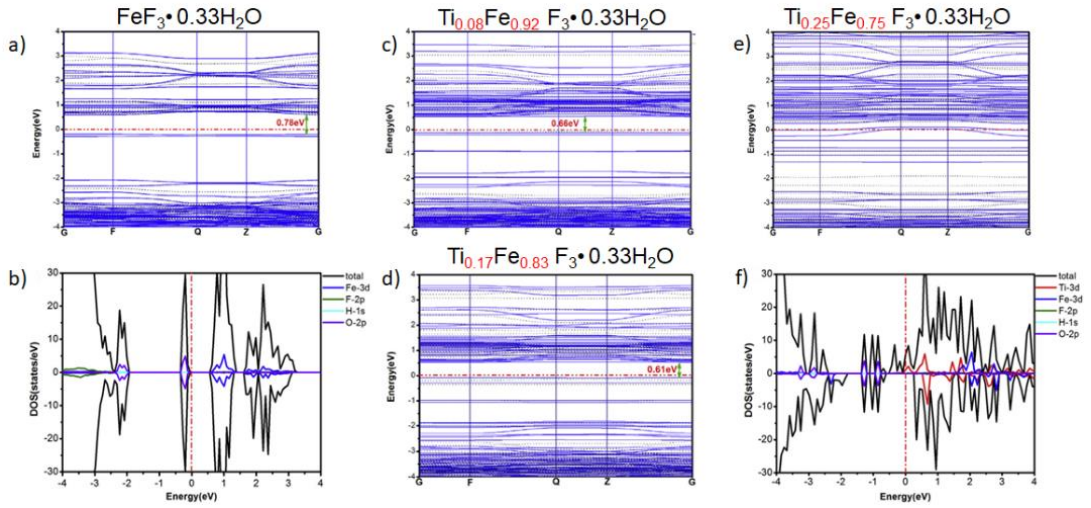

Figure 4.1. Electronic band structure and DOS of a,b) undoped and c,d,e,f) Ti-doped $FeF_3 \bullet 0.33H_2O$[20].

Liu et. al. (2020)[19] performed a study on Ni doping of $FeF_3 \cdot 0.33H_2O$. **Figure 4.2** shows the band structures and DOS of undoped $FeF_3 \cdot 0.33H_2O$ as well as doped $Fe_xNi_yF_3 \cdot 0.33H_2O$. The undoped bandgap is calculated to be 0.918 eV, and the Ni doped structure shows a more significant reduction in bandgap than the Ti doping with the same concentration. **Figures 4,2c,d** show the changes in DOS upon doping, with the vertical red line representing the fermi energy. The effects of the Ni-3d electrons are seen in the red bands of **Figure 4.2d**. The impurity band from the dopant appears at a lower energy than the pure $FeF_3 \cdot 0.33H_2O$ band structure, contributing to improved conductivity overall[19].

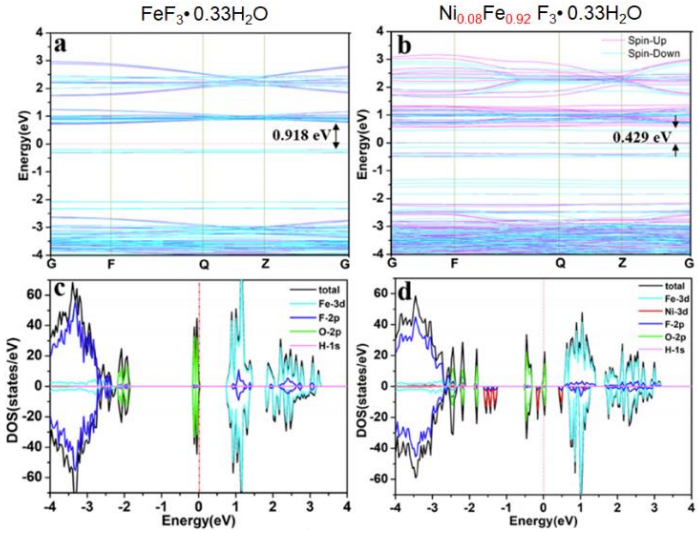

Figure 4.2. Electronic band structure and DOS of a,c) undoped and b,d) Ni-doped $FeF_3 \cdot 0.33H_2O$[19].

Many of these doping studies have also been done experimentally and can corroborate the findings of the computational models. In particular, the Ni-doped and undoped $FeF_3 \cdot 0.33H_2O$ modeled in **Figure 4.2** were implemented in a battery for electrochemical testing. The cycling performance of each cell demonstrates a reversible capacity retention of 161 mAh g^{-1} after 50 cycles for the Ni-doped cathode compared to only 68 mAh g^{-1} for the undoped cathode (**Figure 4.3**). This improvement is attributed to the reduced bandgap that arises from doping and results in fast charge transport within the cell[19].

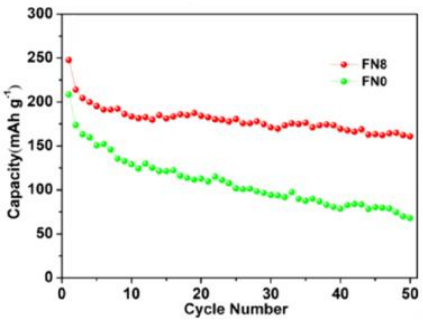

Figure 4.3. Gravimetric cycling performance for doped and undoped $FeF_3 \cdot 0.33H_2O$[19].

Many doping studies involving FeF_3 are done with the hydrate HTB structure mainly due to its improved electrochemical properties compared to the FeF_3 anhydrate on its own. Although the hydrates exhibit improved Li+ insertion, they tend to be unstable in the long-term due to side-reactions occurring between the water molecules and fluoride ions. It would be beneficial to

consider doping the rhombohedral FeF_3 structure instead to inform the synthesis of the FeF_3 C-NFs proposed in previous work (Section 3)[13].

5. Proposal and Experimental Validation

To explore which metal impurities may lead to a smaller bandgap, DFT calculations can be performed. Once appropriate exchange correlation approximations are selected, representative band structures can be calculated from relaxed crystal structures. These crystal structures would be approximations of what we expect to see during synthesis, the rhombohedral FeF_3 structure with a low concentration of selected metal defects. Attention would have to be paid to the formation energies of the defects which may help predict which synthesis options are more realizable. By determining which structures have low formation energies and favorable electronic band structures, we can suggest the best candidates for synthesis.

The previously mentioned FeF_3 CNFs were synthesized by Yushin et. Al (2017)[13] via polymer electrospinning. The synthesis of the FeF_3 CNFs performed here can be adapted to accommodate other transition metals that achieve the desired doping concentration by dissolving that metal in the polymer solution in the first step.

The structural properties of the proposed doped FeF3 and CNFs cathodes can be investigated through imaging techniques. X-ray diffraction (XRD) confirms the formation of FeF_3 nanofibers through characteristic Fe-F bonds and is anticipated to show new metal fluoride (M-F) bonds upon successful synthesis. Scanning electron microscopy (SEM) measurements examine the nanoparticle variation and is anticipated to show how size optimization will enhance the occurrence of tunneling to result in lowered impedance.

The electrochemical properties can be tested by measuring their performance in a functioning cell. Electrochemical impedance spectroscopy (EIS) and voltage profiling measurements were performed for the FeF_3 CNFs discussed in section 3 and should be performed on the cathodes in this work[24]. Stability of the battery components is vital for the long-term use and commercialization of a battery. Performing electrochemical measurements, while repeatedly cycling the battery through charging and discharging is an effective way to test for long-term stability of any battery material and should be done for the proposed doped FeF_3 CNFs. Using EIS can also help to determine the effect of nanoparticle size on charge transfer resistance.

6. Conclusion

We have examined iron (III) fluoride as a promising candidate to replace the cobalt oxide cathodes in modern lithium-ion batteries. Cobalt is problematic more in its sourcing than scarcity and should not be relied upon for the world's future energy. Three different sections contributing to the improvement of iron (III) fluoride based cathode materials are included, discussing the importance of structural stability within the crystal lattice, nanoconfinement as a method for increasing electron mobility and cycle stability, and doping with metal fluoride cathodes as a way of decreasing insulation properties. Based on these sections, an experimental procedure is proposed that may allow for the synthesis of more stable, energy dense, and earth abundant cathodes for modern lithium-ion batteries.

References

1. Pourret, O. & Faucon, M.-P. Cobalt. in *Encyclopedia of Geochemistry: A Comprehensive Reference Source on the Chemistry of the Earth* (ed. White, W. M.) 1–4 (Springer International Publishing, 2017). doi:10.1007/978-3-319-39193-9_271-2.

2. Amnesty International. This is what we die for: Human rights abuses in the democratic republic of the congo power the global trade in cobalt. *Afr 62/3183/2016* 88 (2016).

3. Technische Universtität München, L.-M.-U. M. *e-conversion - Propos. a Clust. Excell.* 1–96 (2018).

4. Danilov, Y. S. Effect of grain size on the Bauschinger effect. *Met. Sci. Heat Treat.* 6, 563–565 (1964).

5. Shamah, A. M., Ibrahim, S. & Hanna, F. F. Formation of nano quasicrystalline and crystalline phases by mechanical alloying. *J. Alloys Compd.* 509, 2198–2202 (2011).

6. Liu, P. *et al.* Crystal structure and mechanical properties of nickel–cobalt alloys with different compositions: A first-principles study. *J. Phys. Chem. Solids* 137, 109194 (2020).

7. Hanawa, T. 1 - Overview of metals and applications. in *Metals for Biomedical Devices* (ed. Niinomi, M.) 3–24 (Woodhead Publishing, 2010). doi:https://doi.org/10.1533/9781845699246.1.3.

8. Davies, W. E. U. S. Geological Survey. *Bioscience* 14, 33–35 (1964).

9. Fu, X. *et al.* Perspectives on Cobalt Supply through 2030 in the Face of Changing Demand. *Environ. Sci. Technol.* 54, 2985–2993 (2020).

10. Consumer Electronics Market Forecast 2026 | Global Report. https://www.gminsights.com/industry-analysis/consumer-electronics-market.

11. Electric Vehicle Market Growth, Industry Trends, and Statistics by 2030 | COVID-19 Impact Analysis | MarketsandMarkets. https://www.marketsandmarkets.com/Market-Reports/electric-vehicle-market-209371461.html#:~:text=The Electric Vehicles Market is,is from 2019 to 2030.

12. Mizushima, K., Jones, P. C., Wiseman, P. J. & Goodenough, J. B. LixCoO2 (0. *Solid State Ionics* 3–4, 171–174 (1981).

13. Wu, F. & Yushin, G. Conversion cathodes for rechargeable lithium and lithium-ion batteries. *Energy Environ. Sci.* 10, 435–459 (2017).

14. Li, R. F., Wu, S. Q., Yang, Y. & Zhu, Z. Z. Structural and electronic properties of Li-ion battery cathode material FeF3. *J. Phys. Chem. C* 114, 16813–16817 (2010).

15. Frey, P. A. & Reed, G. H. The Ubiquity of Iron. *ACS Chem. Biol.* 7, 1477–1481 (2012).

16. Conte, D. E. & Pinna, N. A review on the application of iron(III) fluorides as positive electrodes for secondary cells. *Mater. Renew. Sustain. Energy* 3, (2014).

17. Li, C., Gu, L., Tsukimoto, S., Van Aken, P. A. & Maier, J. Low-temperature ionic-liquid-based synthesis of nanostructured iron-based fluoride cathodes for lithium batteries. *Adv. Mater.* 22, 3650–3654 (2010).

18. Chen, D. *et al.* Modifying the size and shape of monodisperse bifunctional alkaline-earth fluoride nanocrystals through lanthanide doping. *J. Am. Chem. Soc.* 132, 9976–9978 (2010).

19. Liu, M. *et al.* Band-Gap Engineering of FeF3·0.33H2O Nanosphere via Ni Doping as a High-

Performance Lithium-Ion Battery Cathode. *ACS Sustain. Chem. Eng.* 8, 15651–15660 (2020).

20. Yang, Z. *et al.* First-principles study of Ti doping in FeF3·0.33H2O. *Curr. Appl. Phys.* 16, 905–913 (2016).

21. Wang, F. *et al.* Tracking lithium transport and electrochemical reactions in nanoparticles. *Nat. Commun.* 3, 1–8 (2012).

22. Badway, F., Cosandey, F., Pereira, N. & Amatucci, G. G. Carbon Metal Fluoride Nanocomposites. *J. Electrochem. Soc.* 150, A1318 (2003).

23. Li, L., Meng, F. & Jin, S. High-capacity lithium-ion battery conversion cathodes based on iron fluoride nanowires and insights into the conversion mechanism. *Nano Lett.* 12, 6030–6037 (2012).

24. Fu, W. *et al.* Iron Fluoride–Carbon Nanocomposite Nanofibers as Free-Standing Cathodes for High-Energy Lithium Batteries. *Adv. Funct. Mater.* 28, 1–8 (2018).

25. Ni, D. *et al.* Improved rate and cycling performance of FeF2-rGO hybrid cathode with poly (acrylic acid) binder for sodium ion batteries. *J. Power Sources* 413, 449–458 (2019).

26. Kwon, C. W. *et al.* Nanocrystalline Materials For Lithium Batteries. *New Trends Intercalation Compd. Energy Storage* 439–446 (2002) doi:10.1007/978-94-010-0389-6_28.

27. Lukiyanets, B. A., Matulka, D. V. & Grygorchak, I. I. Quantum mechanic tunneling and efficiency of Faraday current-generating process in porous nanostructures. *Condens. Matter Phys.* 14, 1–12 (2011).

28. Bai, Y. *et al.* Understanding the combined effects of microcrystal growth and band gap reduction for Fe(1-x)TixF3 nanocomposites as cathode materials for lithium-ion batteries. *Nano Energy* 17, 140–151 (2015).

29. Allen, P. B. Elementary Solid State Physics: Principles and Applications by M. A. Omar . *Am. J. Phys.* 43, 265-268 (1975).